

A Study of Excitation Energy Deposition

Using the Texas A&M Neutron Ball

Stan Anderson

University Undergraduate Fellow, 1989-90

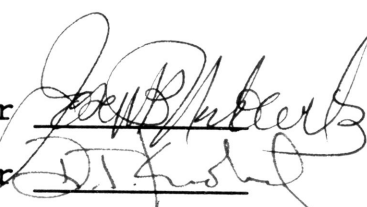
Texas A&M University

Department of Physics

APPROVED

Fellows Advisor

Honors Director

The image shows two handwritten signatures in black ink. The top signature is for the Fellows Advisor and the bottom signature is for the Honors Director. Both signatures are written over horizontal lines that serve as baselines for the text.

## ABSTRACT

### "A Study of Excitation Energy Deposition Using the Texas A&M Neutron Ball"

by Stan Anderson

A test run of a new  $4\pi$  neutron detector has been performed, studying the collisions of 30 Mev/u  $^{14}\text{N}$  with  $^{109}\text{Ag}$  and  $^{60}\text{Ni}$ . Average neutron multiplicities of the two reactions were determined after correction for background effects and the efficiency of the detector. The observed multiplicities were much higher than the anticipated numbers, in the best efficiency Ag case,  $\bar{M}$  ranged from 5.6 to 6.8. An explanation for the lost neutrons has also been explored, but cannot account for all of them. Another test of the neutron detector is now underway.

## TABLE OF CONTENTS

TITLE PAGE . . . . .	i
ABSTRACT . . . . .	ii
LIST OF ILLUSTRATIONS . . . . .	iv
I. SUMMARY . . . . .	1
II. EXPLANATION OF RESEARCH TOPIC . . . . .	3
III. DESCRIPTION OF EXPERIMENT . . . . .	4
IV. CALIBRATIONS . . . . .	8
A. <u>Neutron Multiplicity</u> . . . . .	8
B. <u>Timing Calibration</u> . . . . .	15
C. <u>Energy Calibration</u> . . . . .	16
V. Ag AND Ni MULTIPLICITY RESULTS . . . . .	18
VI. ACCOUNTING FOR LOST NEUTRONS . . . . .	21
VII. CONCLUSIONS AND FUTURE PLANS . . . . .	26
REFERENCES . . . . .	28

## LIST OF ILLUSTRATIONS

### Figures

Figure 1.	The Neutron Ball neutron detector.	5
Figure 2.	A diagram of the experimental setup.	5
Figure 3.	A block diagram of the counting electronics.	7
Figure 4.	A sample $^{252}\text{Cf}$ neutron multiplicity distribution and background distribution	10
Figure 5.	A sketch of the fit to Figure 4a.	11
Figure 6.	Final $^{252}\text{Cf}$ neutron multiplicity distribution fits with background corrected distributions.	13
Figure 7.	Background corrected neutron multiplicity distribution taken from an ORNL report.	15
Figure 8.	Sample energy versus time plot taken from the residue detector.	17
Figure 9.	Neutron multiplicity distribution fit to Ni data using one Gaussian.	19
Figure 10.	Neutron multiplicity distribution fits to Ni and Ag data using two Gaussians.	19
Figure 11.	Sample neutron capture time distributions.	22
Figure 12.	Total neutron capture time distribution and fit from Ni data.	24
Figure 13.	Total neutron capture time distribution and fit from Ag data.	25

### Tables

Table 1.	Experiment Setup Descriptions.	11
Table 2.	Parameters for $^{252}\text{Cf}$ Multiplicity Distribution Fit.	13
Table 3.	Corrected Average Multiplicities Ni and Ag Data, Setups #2 and #4.	21
Table 4.	Parameter Values for Capture Time Distribution Fits.	23

## I. SUMMARY

The purpose of this research project was to examine the velocity distributions of evaporation residues produced in a heavy ion collision. My goal was to quantify the statistical spreading of the final residue velocities, and to try to establish correlations between the initial excitation energies and the final residue velocities. Using the new Neutron Ball neutron detector, an experiment was run at the Cyclotron Institute in which we detected the neutrons emitted by deexciting residues. After our initial analysis, it was decided to refocus our study away from the residue velocities, and look instead at the actual numbers of neutrons detected in the experiment.

Three different calibrations of the experimental data had to be performed, involving the neutron multiplicity distributions, the residue times of flight, and the residue energies. A  $^{252}\text{Cf}$  source was used to test the detection response of the Neutron Ball. Corrections were made to the observed distributions for background effects and for the efficiency of the Neutron Ball. Timing and energy calibrations were also performed by utilizing particle punch through points on energy versus time plots derived from the residue detector used in the experiment.

Background corrected multiplicity distributions were then produced from the Ag and Ni target data in the experiment. The efficiency corrected averages of these distributions turned out to be much lower than anticipated; in the case of the Ag data, by a factor of two. An estimation was then made of the numbers of

neutrons escaping the counting gate, which was too low to account completely for the missing neutrons. Currently, Dr. Natowitz's research group is performing a second test of the Neutron Ball to try to better understand its response.

## II. EXPLANATION OF RESEARCH TOPIC

Studies in nuclear physics often involve the collision of a projectile nucleus, accelerated by a cyclotron, with a target nucleus. For a brief instant after a central collision, the two nuclei exist together in a combined system. In some nuclear reactions, there is a tendency for this highly excited combined system to fission into two relatively large pieces. While in other reactions, there is a tendency for the combined system, or compound nucleus, to get rid of its excess energy through a process of evaporation of nucleons. In reactions involving the more massive nuclei, the emitted particles are primarily neutrons with smaller numbers of protons and alpha particles.

It is quite easy to measure the velocity of the residual nucleus, or residue, that is left over. And if there were no evaporation of protons and neutrons from the compound nucleus, this would provide the excitation energy of the compound system. Since there is an evaporative process, however, compound nuclei which start out at the same excitation energy may not end up with the same final velocities.

Hence, measuring a specific final velocity for several residues does not necessarily give you a group of similarly excited compound nuclei. It was the goal of this research project to measure the number of neutrons emitted by the deexciting residues, and to get a handle on the statistical spreading of final velocities of similarly excited compound nuclei. We were also hoping to study correlations between the

initial excitation energies of the residues and their final velocities.

After performing an experiment in October of 1989 with the new Neutron Ball neutron detector at the Cyclotron Institute, it was necessary in the subsequent data analysis to redirect the study. Two particular reactions were used in the experiment, involving a nitrogen beam on silver and nickel targets. In the case of the silver data, we found neutron counts that were approximately two times too low. This reaction is thought to have a fairly well understood deexcitation scheme, and so our further analysis focused on ways to account for the lost neutrons.

### III. DESCRIPTION OF EXPERIMENT

I was fortunate to be able to participate with Dr. Natowitz's research group in an experiment performed between October 2-7, 1989, at the Cyclotron Institute. The purpose of the experiment was to detect the neutrons emitted by evaporation residues utilizing the Neutron Ball, a large spherical neutron detector shown in Figure 1. Two different collisions were used in the experiment;  $^{14}\text{N} + ^{109}\text{Ag}$  and  $^{14}\text{N} + ^{60}\text{Ni}$ , both at nitrogen beam energies of 30 Mev/u. A diagram of the experimental setup is shown in Figure 2.

The Neutron Ball consists of a spherical shell of approximately 1.5 meters in diameter, and is divided into upper



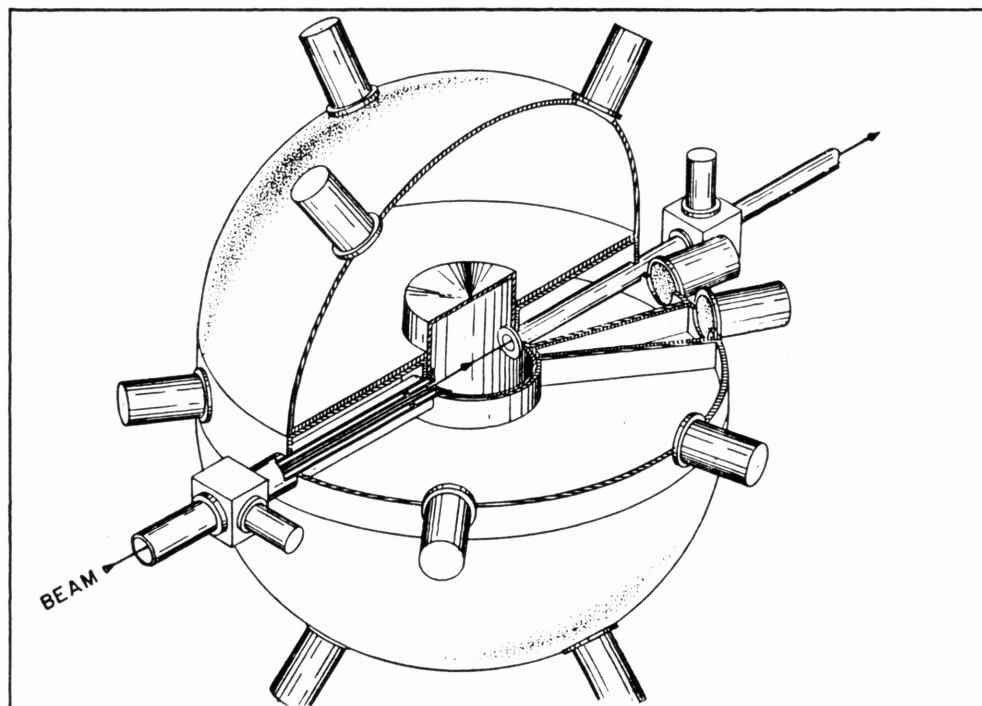


Figure 1. The Neutron Ball neutron detector.

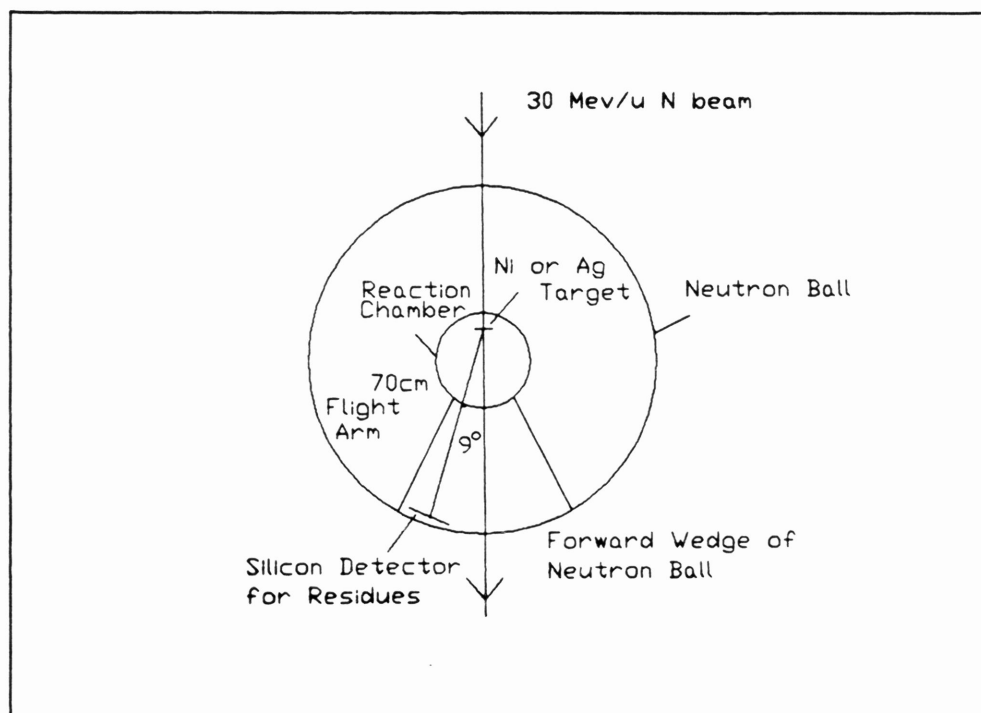


Figure 2. A diagram of the experimental setup.

and lower hemispheres, surrounding a cylindrical reaction chamber case. There are also 10 hollow equatorial wedges. The Ball is filled with a pseudo cumene liquid scintillator, which is mixed with a given percentage by weight of gadolinium, in our case 0.2% by weight. The scintillator emits light in response to the capture of thermalized neutrons.<sup>1</sup> The shell of the Neutron Ball is fitted with photomultiplier tubes which detect and amplify the light signals emitted by the scintillator.

Neutrons are detected by the instrument after a reaction through a process of elastic scattering with protons in the liquid. The neutrons are eventually slowed down enough to be captured by the Gd nuclei in the liquid scintillator. The Gd nuclei then deexcite by emitting a capture gamma ray, bringing about a light flash from the scintillator which the phototubes then detect.<sup>1</sup>

Also shown in Figure 2. is the  $300\mu$  thick silicon detector used for detecting the residues in the experiment. The detector consists of four separated quadrants and was placed at  $9^\circ$  to the beam direction in the forward wedge of the Neutron Ball. A veto counter was also included behind the residue detector to discriminate the residues from the higher energy lighter particles passing all the way through the residue detector.

Shown in Figure 3. is a diagram of the electronics used in the neutron counting. Pulses were taken from the Neutron Ball's upper and lower hemispheres and from the equatorial wedge segments. These signals were first run through a constant fraction discriminator to set a requirement on the number of

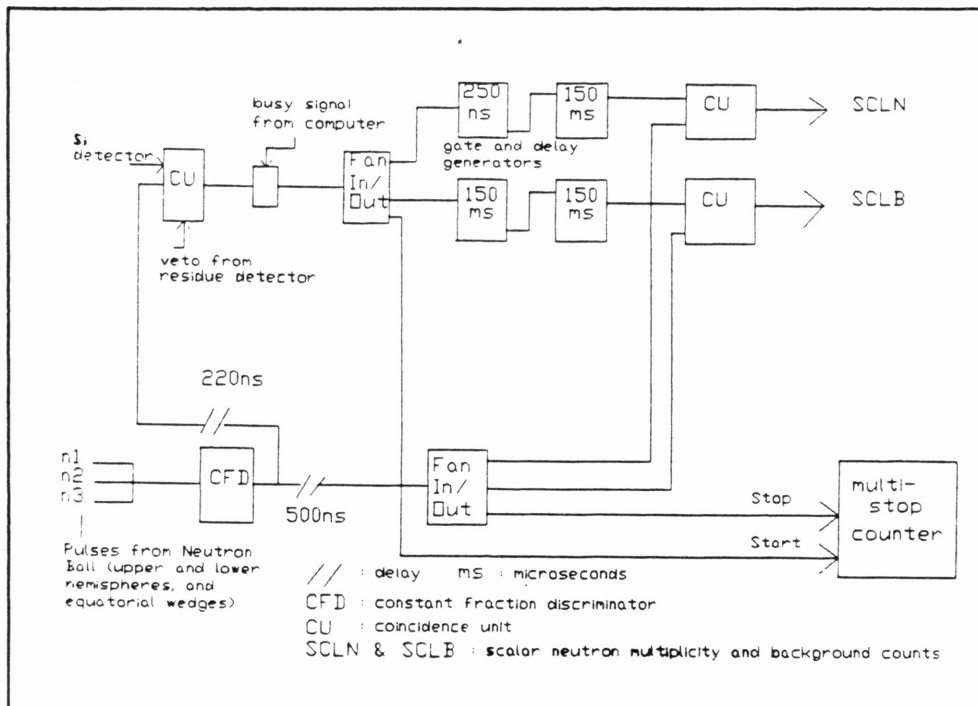


**Figure 3.** A block diagram of the counting electronics.

neutrons detected for an accepted event. The number of neutrons that a residue emits is known as the residue's neutron multiplicity. At different times in the experiment, we examined events with  $M \geq 2$  and  $M \geq 1$ .

Coincidences were then taken with the silicon residue detector, to count only the neutrons emitted by deexciting compound nuclei. Within two separate counting gates, the neutron multiplicity for an event was recorded (SCLN), followed by a background count (SCLB). The neutron multiplicity counting gate was  $150 \mu\text{s}$  long, and was triggered by the prompt pulse signal from the Neutron Ball at the start of the event. Immediately after this counting gate, the  $150 \mu\text{s}$  background counting gate was opened to record background multiplicities.

A special Multi-Stop Counter was also used to measure the individual neutron capture time distributions. In other words, this unit recorded the time of capture, after opening the counting gate, for the 1st captured neutron, the 2nd neutron, etc. Times were recorded for all the neutrons detected in an event. So the parameters taken in the experiment included this timing information, energy information for the residues derived from the residue detector, and the number of neutrons emitted by the individual residues.

#### IV. CALIBRATIONS

As in all nuclear studies, raw information from an experiment has to be converted into meaningful values. For example, the raw timing information must be converted into nanoseconds, and energy data into units of Mev. The work on the data analysis has included the following calibrations:

##### A. Neutron Multiplicity

I first worked on the calibration for the neutron multiplicity distributions. To get a feel for how the Ball would respond in this experiment, we looked at the multiplicity distributions from a known  $^{252}\text{Cf}$  source. The first step in calculating an average multiplicity from the data is to correct the experimental count for the background counts that are added in. To derive a fit to the data, we first assumed a Gaussian shape for the background corrected multiplicity distribution. We

then added in percentages of the total background count to each given multiplicity in the assumed form, to "smear" the assumed Gaussian into the experimental distribution. As an example, if the background distribution consisted of 50% multiplicity 0 and 50% multiplicity 1 counts, then for precisely half of the events, you would need to add 1 count to each given multiplicity in the assumed Gaussian form to fold it into the experimental distribution.

The actual fitting procedure involved a least-squares fit to the data, using the dispersion, normalization, and average multiplicity of the assumed Gaussian as free parameters. The functional form was

$$H(M) = \frac{N}{\sqrt{2\pi}\sigma} \exp\left[-\frac{(M-\bar{M})^2}{2\sigma^2}\right], \quad (1)$$

where  $\sigma$  is the dispersion,  $N$  the normalization, and  $\bar{M}$  the average of the assumed distribution. An example of one of the  $^{252}\text{Cf}$  neutron multiplicity distributions is shown along with its background distribution in Figure 4. And a sketch of the derived fit, using the above unfolding procedure, is shown in Figure 5.

During the experiment, we used two different multiplicity requirements set with the constant fraction discriminator (either  $M \geq 2$  or  $M \geq 1$ ), and we used two different groups of voltage threshold settings on the phototubes of the Neutron Ball to try to find the optimal combination of settings. Each of these settings was called a "Setup," and these are further explained in Table 1.

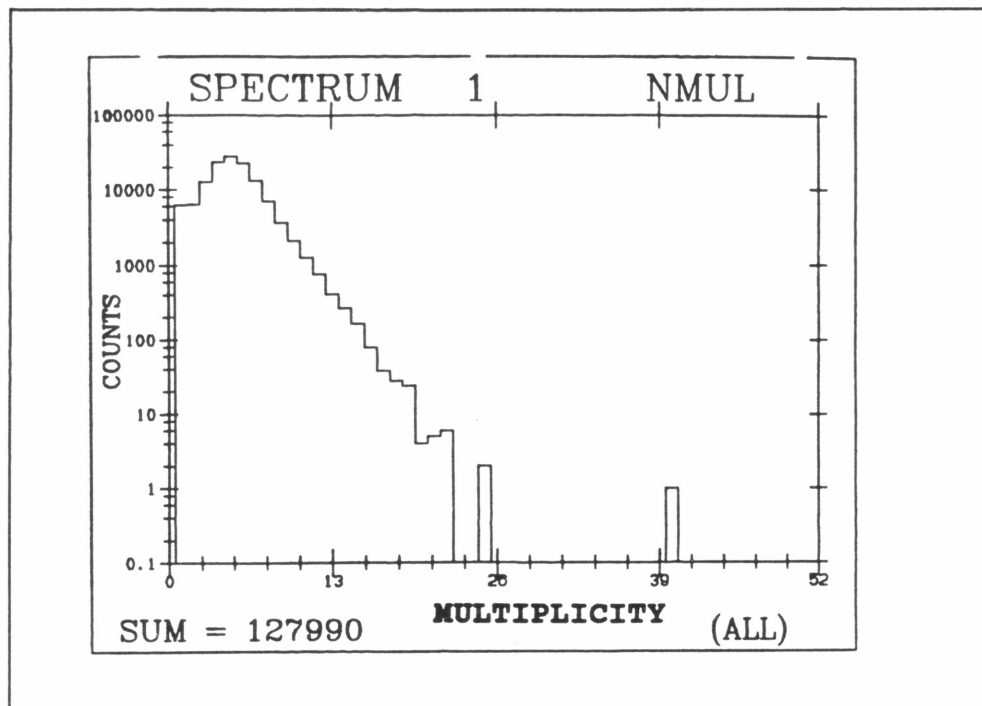


Figure 4a. A sample  $^{252}\text{Cf}$  neutron multiplicity distribution uncorrected for background.

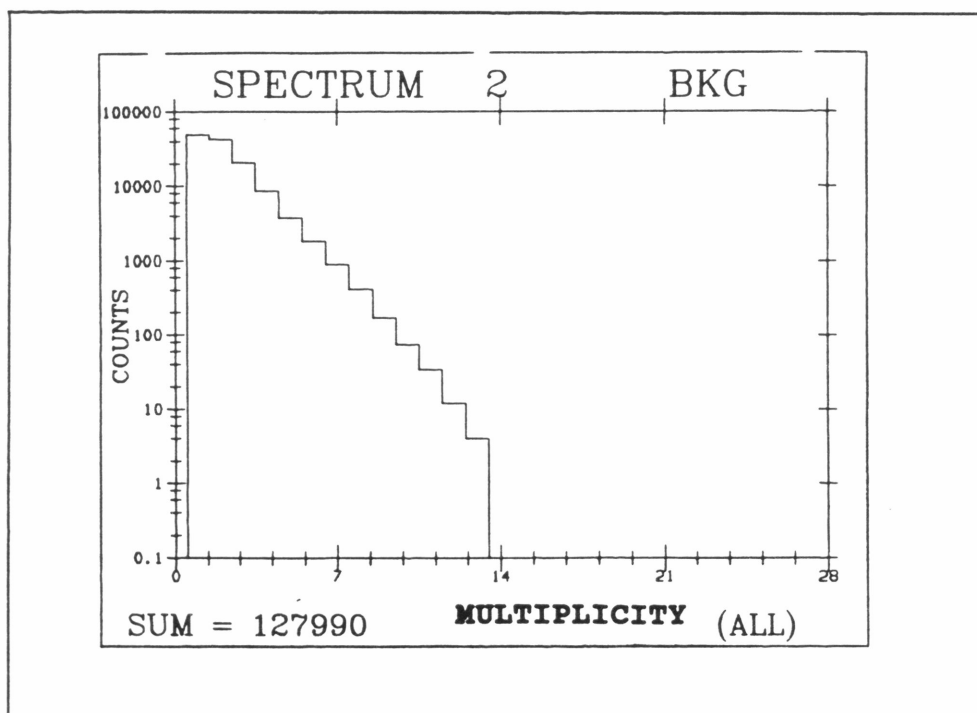


Figure 4b. The corresponding background distribution for Figure 4a.

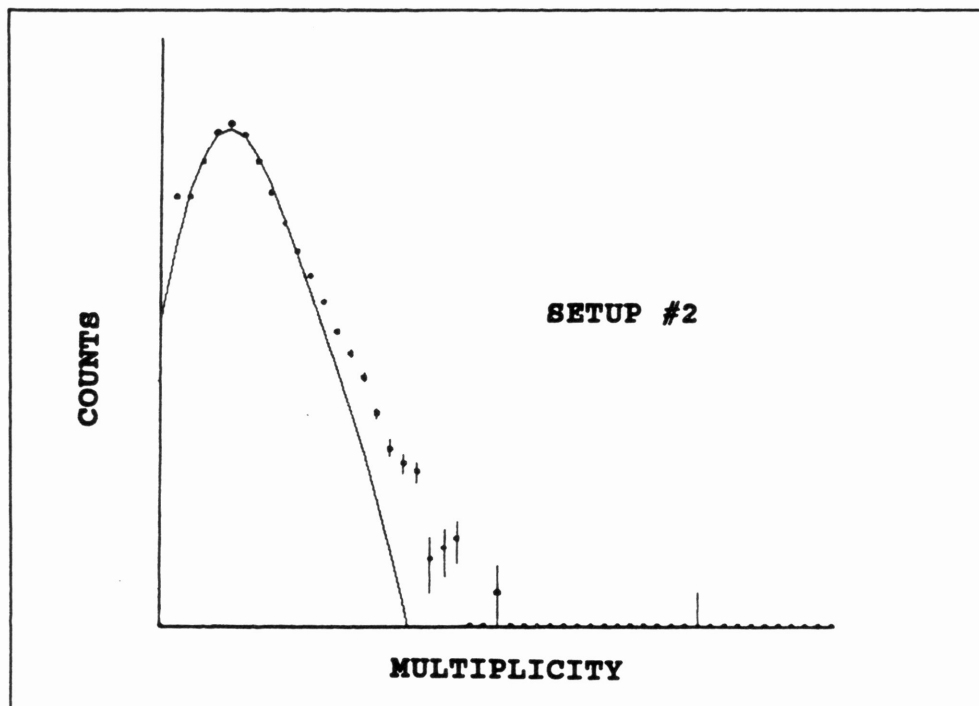


Figure 5. A rough sketch (log. plot) of the fit to the Figure 4. distribution using the unfolding procedure.

Table 1.

Experiment Setup Descriptions

Setup #	multiplicity requirement (M)	phototube thresholds
1	$M \geq 2$	high
2	$M \geq 2$	low
3	$M \geq 1$	low
4	$M \geq 1$	high

The above multiplicity distribution fit was for Setup #2. During our multiplicity calibration, we also ran with Setup #4; however, we did have some trouble fitting both distributions at the higher multiplicities. So instead of assuming a single Gaussian distribution for the background corrected distributions, we added two Gaussian forms together for the corrected distribution. The second Gaussian was a broad distribution, and had a small normalization to more easily fit the higher multiplicities. So the functional form was changed to

$$H(M) = \frac{N_1}{\sqrt{2\pi}\sigma_1} \exp\left[-\frac{(M-\overline{M}_1)^2}{2\sigma_1^2}\right] + \frac{N_2}{\sqrt{2\pi}\sigma_2} \exp\left[-\frac{(M-\overline{M}_2)^2}{2\sigma_2^2}\right], \quad (2)$$

where, during the least-squares fit, the six free parameters were the normalization, dispersion, and average multiplicity of both distributions. The final fit for the two setups used in the  $^{252}\text{Cf}$  calibration is shown in Figure 6. The parameters found for the final Gaussian forms, along with the averages of the complete distributions is presented in Table 2. The averages found using a two Gaussian fit differed by less than 1% from the averages found using the one Gaussian fit.

The fitting routine with two Gaussian distributions does provide a better fit. However, we have no physical explanation for the extra component at the higher multiplicities. I was able to find a background corrected  $^{252}\text{Cf}$  distribution, published by Spencer, et. al. from the Oak Ridge National Laboratory.<sup>2</sup> Using the functional form (2) I made a least-squares fit to this



Table 2.  
Parameters for  $^{252}\text{Cf}$  Multiplicity Distribution Fit

Setup	$\sigma_1$	$M_1$	$N_1$	$\sigma_2$	$M_2$	$N_2$	$M$
#2	1.56	4.00	1.22 $\times 10^5$	3.00	9.44	2730	3.03
#4	1.81	2.82	1.07 $\times 10^5$	12.3	17.8	1500	2.84

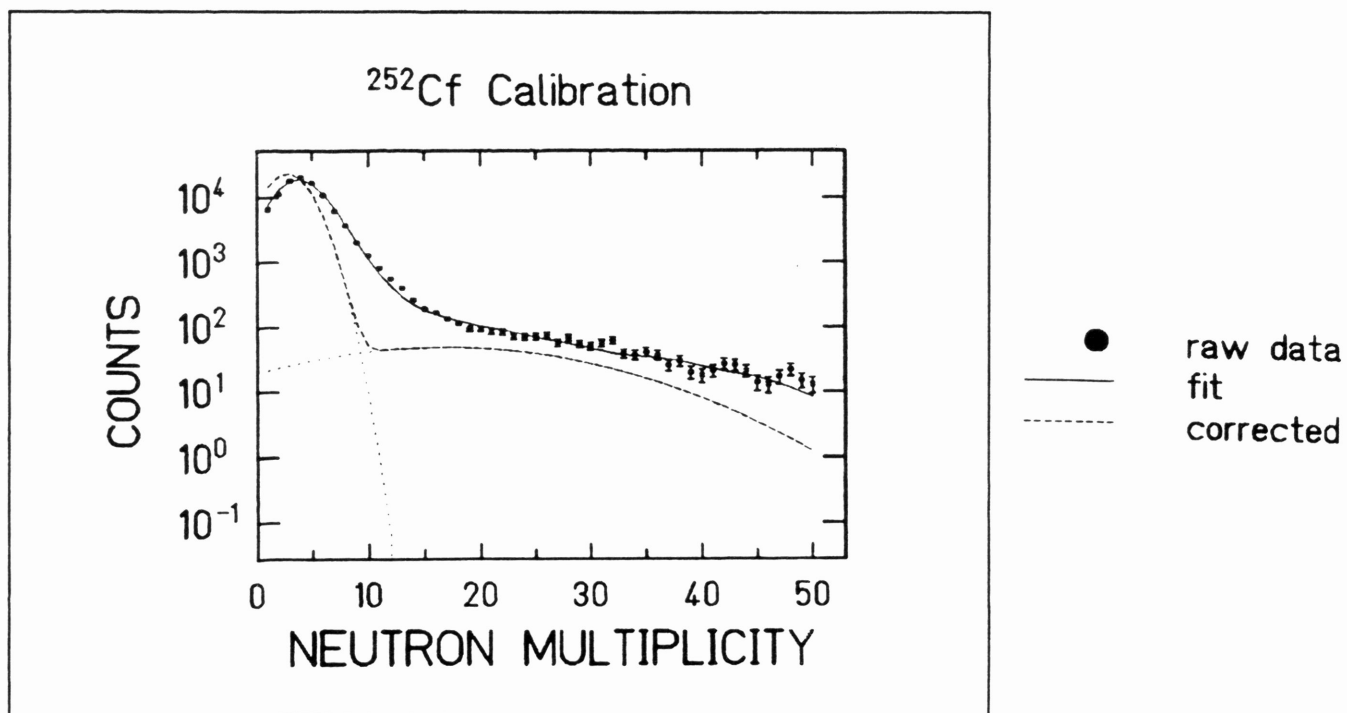


Figure 6a.  $^{252}\text{Cf}$  Setup#2 neutron multiplicity distribution fit, showing the background corrected distribution, with the two composite Gaussians in the lighter dotted lines.

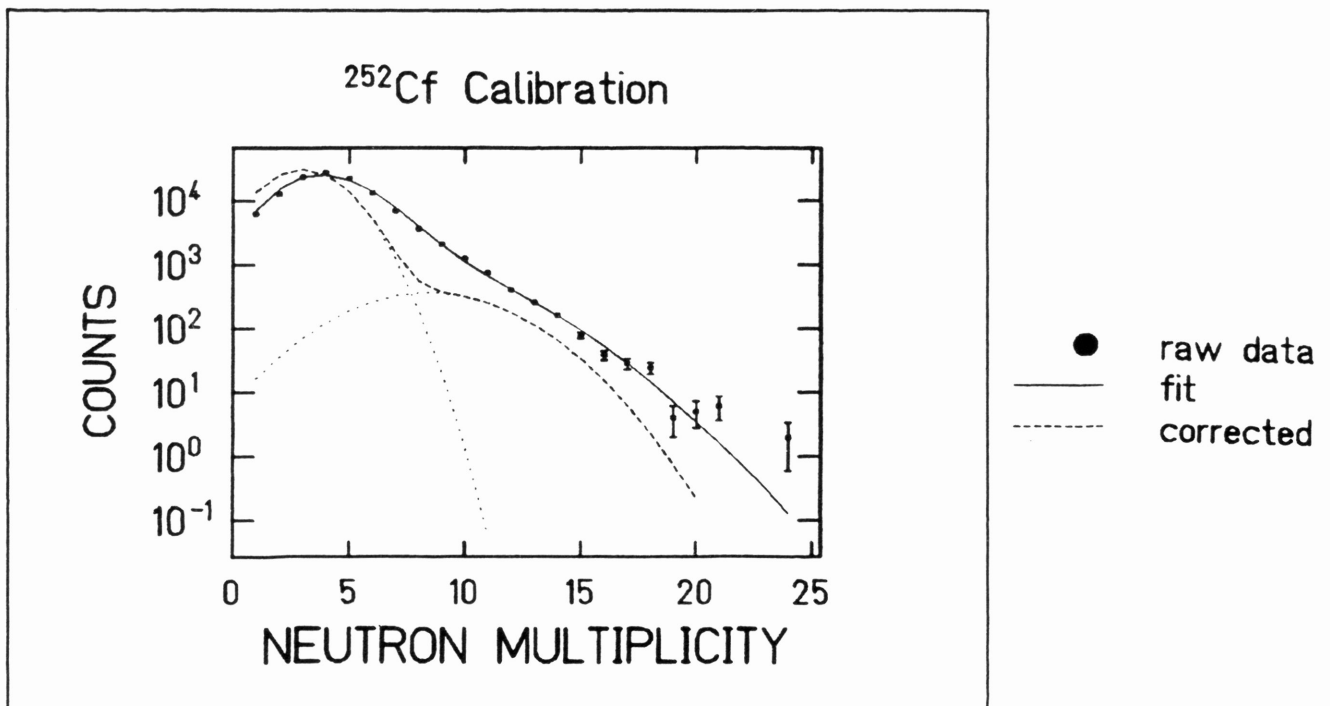


Figure 6b. <sup>252</sup>Cf Setup #4 neutron multiplicity distribution fit, showing the background corrected distribution, with the two composite Gaussians in the lighter dotted lines.

background corrected data in Figure 7. As you can see, the second Gaussian form, at the higher average multiplicity, has not moved as far to the right as in our fit attempts. This discrepancy is something we still do not understand.

By knowing the actual average of the <sup>252</sup>Cf distribution,  $\bar{M}=3.773 \pm .007$ , we were next able to derive some rough efficiency values for the Neutron Ball. The idea was to again use an assumed Gaussian form for the efficiency corrected real neutron multiplicity distribution, and fold this, through the binomial response of the detector, into the background corrected distribution. There were again three free parameters for the assumed functional form; however, this time the average

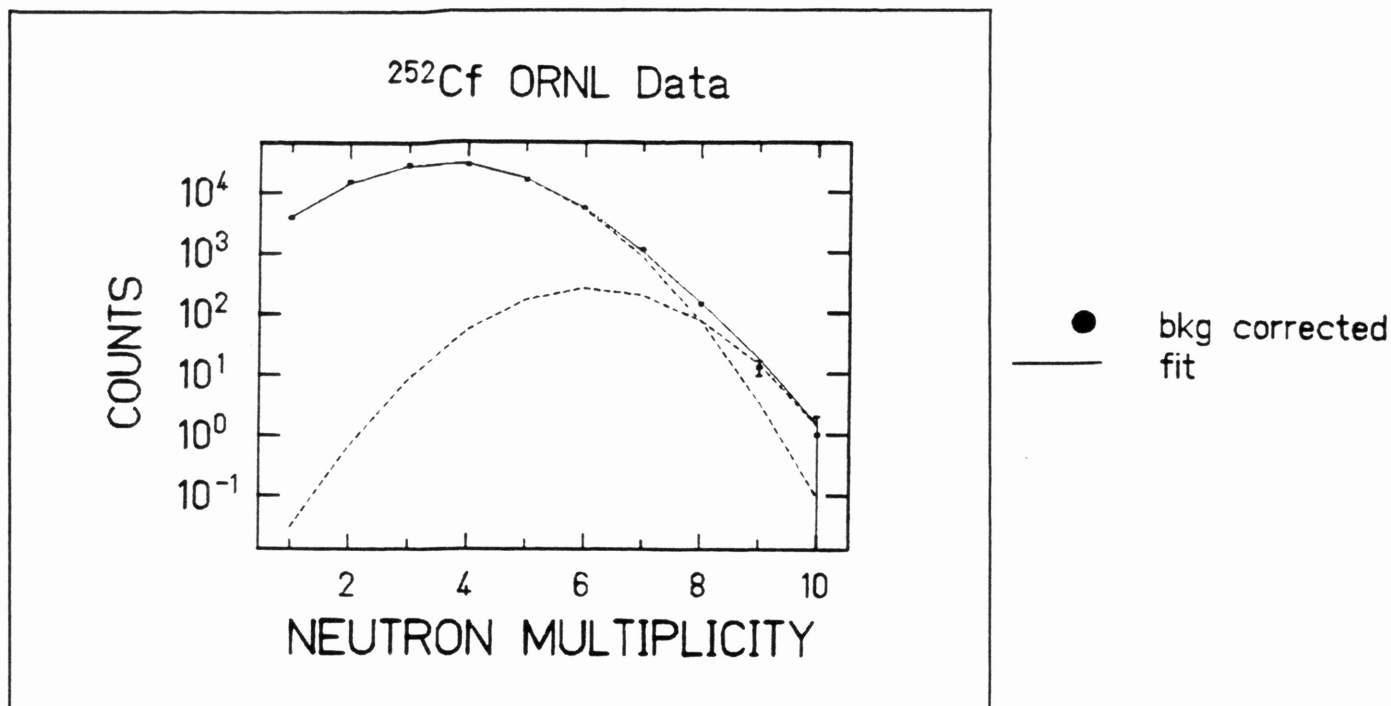


Figure 7. Decomposition of ORNL neutron multiplicity distribution into two Gaussian distributions.<sup>2</sup>

multiplicity was fixed at  $\bar{M} = 3.773$ , and the third free parameter became the efficiency of the Neutron Ball. The unfolding procedure resulted in detection efficiency values of approximately .847 and .810 for Setup #2 and Setup #4 respectively. It would appear that the optimal settings for using the Ball would correspond to Setup #2, with multiplicity requirement  $M \geq 2$  and phototube thresholds set low.

#### B. Timing Calibration

To determine the velocities of the detected residues, we needed their times of flight, or the time it took for the residues to arrive at the detector from the target. The raw timing information provided by the residue detector had to be

calibrated into real times. To derive the slope of this timing calibration (the number of nanoseconds per raw timing channel), a 10ns delay was inserted into the electronics of the experiment. This provided a definite shift in the peaks of graphics plots made of the timing information, and gave us the slope of the calibration. To provide an intercept for the timing calibration, one known time of flight had to be used. We were able to use a specific point on an energy versus time plot derived from the residue detector, shown in Figure 8.

The point marked is the alpha particle "punch-through" point, the point at which fast alpha particles produced in the reactions just barely pass through the silicon residue detector. This takes place at a fixed alpha particle energy for a given thickness of silicon detector (in our case, 24.3 Mev alpha particles.) From this energy, we knew the velocities of the "punch-through" alphas. Since we knew the distance from the residue detector to the target (70cm), we then knew the time of flights of the alpha particles. This provided the intercept for the timing calibration. A timing calibration was performed on three of the four quadrants of the residue detector. The energy versus time plot of the final quadrant was too poor to provide a correct calibration.

### C. Energy Calibration

An energy calibration of the residue detector was performed by Dennis Utley, utilizing the alpha particle and proton

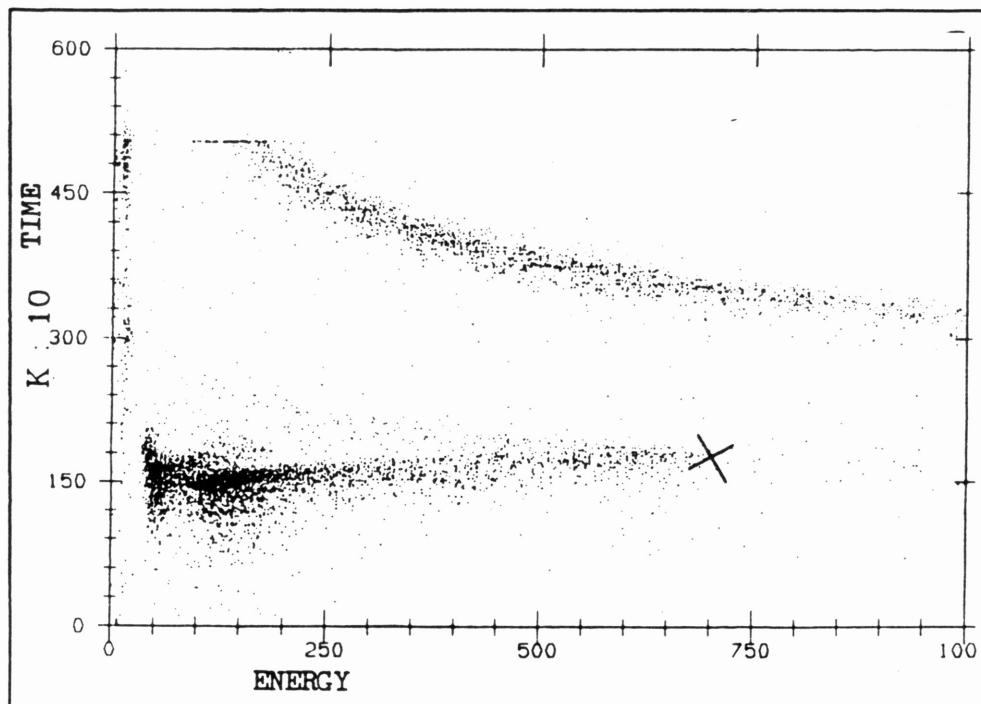


Figure 8. Sample energy versus time plot taken from the residue detector.

punch-through points on the energy versus time plots of the three better quadrants. These two points provided the slope and intercept for the energy calibration. This calibration was then also compared to the energy distribution obtained from the  $^{252}\text{Cf}$  calibration, using the large 79.4 Mev and 103.8 Mev Cf fission fragment peaks.

Energy calibrations are usually not performed with punch-through points, instead one would normally use peaks in a distribution, like the  $^{252}\text{Cf}$  peaks. In our case, however, there were some imprecise voltage gain changes made to the silicon residue detector, and Dennis could only use these peaks as a rough double check.

## V. Ag AND Ni MULTIPLICITY RESULTS

The unfolding procedure described above for deriving the background corrected  $^{252}\text{Cf}$  neutron multiplicity distribution was also applied to the Ag and Ni target data. Data was taken in coincidence with the residue detector, gated to pick up only the residues. In the first part of our analysis, a single Gaussian was again assumed for the background corrected distribution. However, to derive the fit, we did not look at all of the data at once. The residues that we detected had a distribution of velocities, with the upper cut-off at slightly above the velocity of a full momentum transfer in the collision. We examined the neutron multiplicity distributions of three separate cuts in the residue velocity distributions; having  $V_{\text{res}} > 90\%$ ,  $70\% < V_{\text{res}} < 90\%$ , and  $V_{\text{res}} < 70\%$  of the velocity corresponding to the full momentum transferred.

Again, there were often problems with fitting the higher neutron multiplicities in each of the velocity cuts. We later reexamined several of the fits, and repeated the least-squares calculation with two Gaussian distributions. Just as in the  $^{252}\text{Cf}$  calibration, several different setup numbers were tried, with differing phototube thresholds and multiplicity requirements. A single Gaussian fit for a Ni Setup #2 run is shown in Figure 9. While two Gaussian fits for Ni and Ag Setup #2 runs are shown in Figure 10. The velocity cuts are different in the two examples.

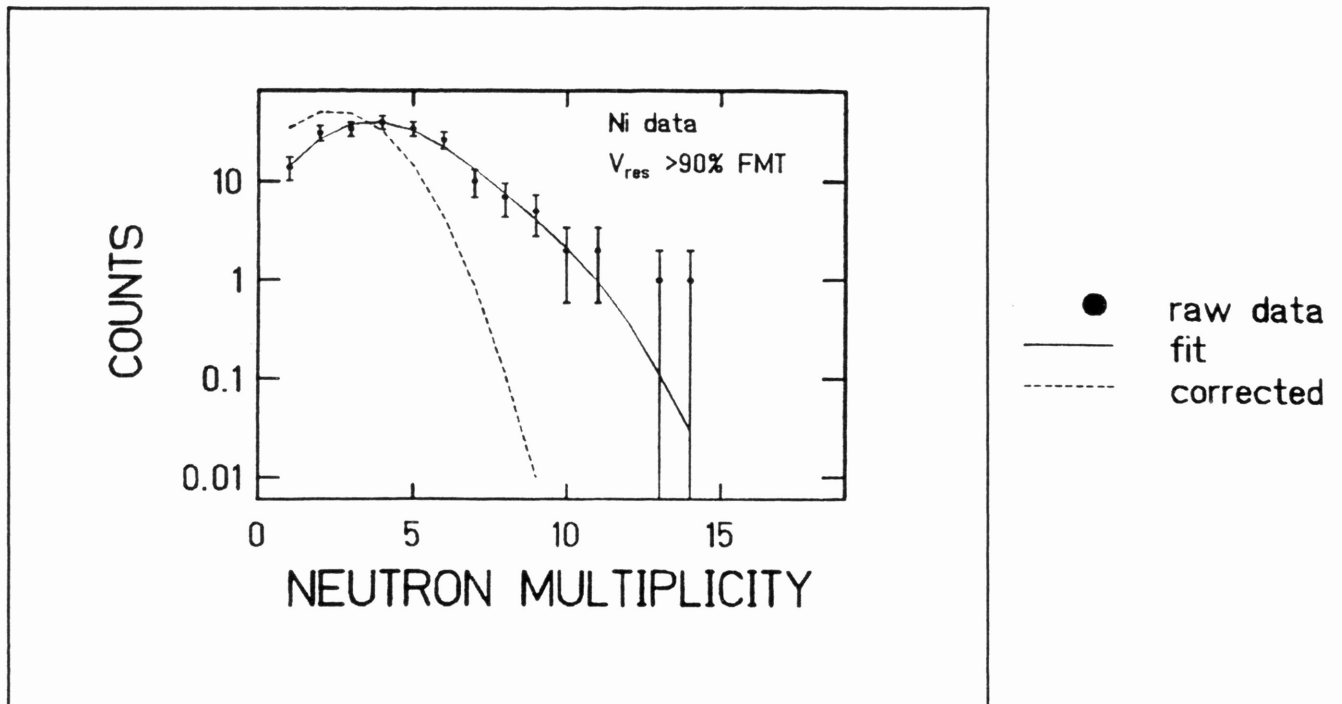


Figure 9. Fit to neutron multiplicity distribution using one Gaussian, taken from a Ni Setup #2 run.

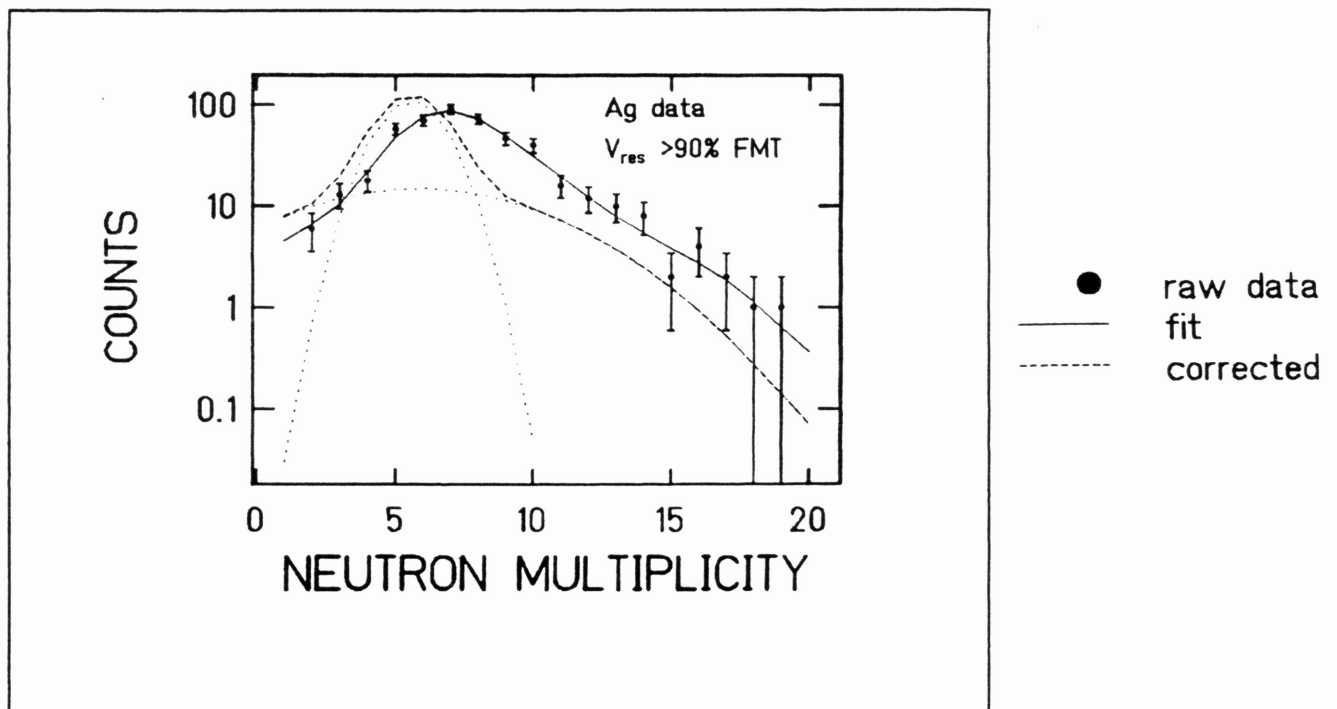


Figure 10a. Fit to neutron multiplicity distribution using two Gaussians, taken from a Ag Setup #2 run.

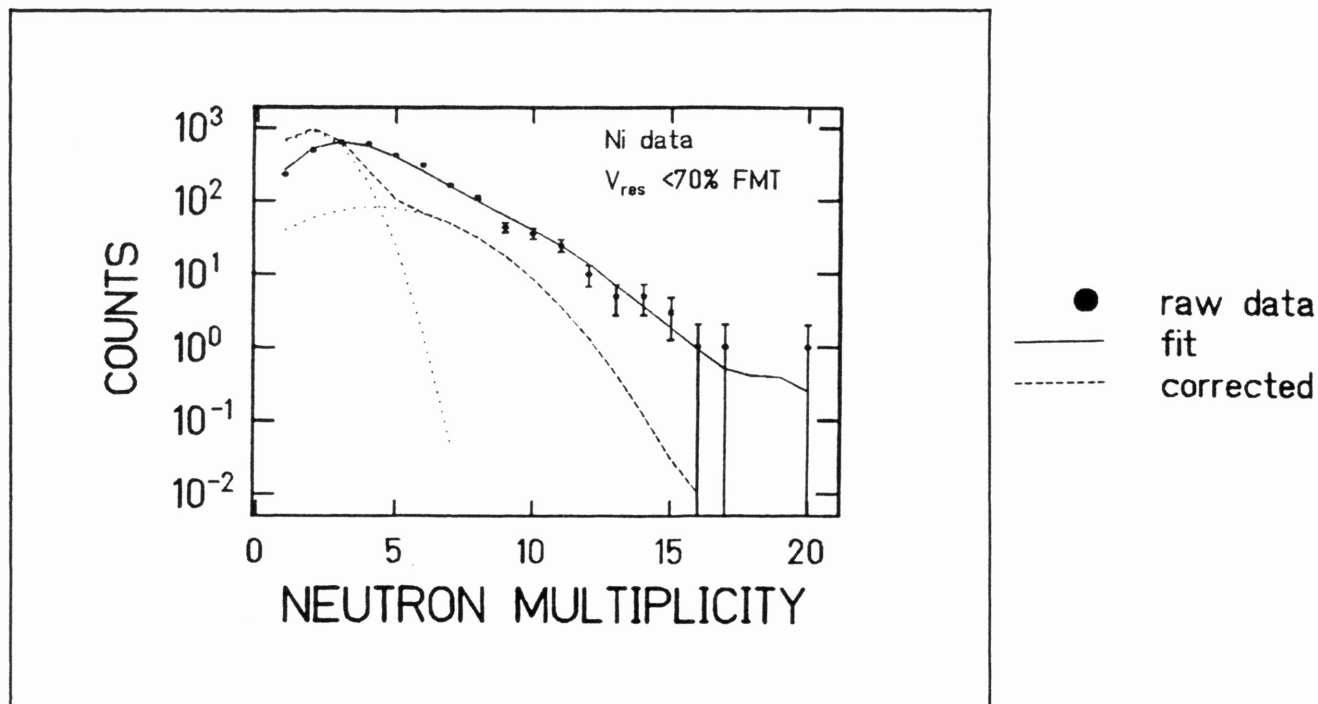


Figure 10b. Fit to neutron multiplicity distribution using two Gaussians, taken from a Ni Setup #2 run.

Dennis Utley performed the statistical calculations on the individual multiplicity distributions, always using the single Gaussian background corrected distributions. Using the efficiency values that were found in the  $^{252}\text{Cf}$  calibration, the background corrected and efficiency corrected average multiplicity values were found; these are presented in Table 3.

These results differ markedly from those obtained in a statistical model calculation which Dennis was also able to run, using the program CASCADE.<sup>3</sup> They also differ markedly from experiments performed in the same mass and energy range by Dr. Natowitz's group.<sup>4</sup> It seems in the case of the Ag data, about one-half of the neutrons are unaccounted for in our analysis.



Table 3.  
Corrected Average Multiplicities  
Ni and Ag Data, Setups #2 and #4

Setup #	Target	$V_{res} < 70\%$	$70\% < V_{res} < 90\%$	$V_{res} > 90\%$	$\epsilon$ eff.
2	Ag	$5.6 \pm .2$	$6.6 \pm .2$	$6.8 \pm .3$	.847
4	Ag	$5.6 \pm .2$	$6.5 \pm .3$	$7.0 \pm .4$	.810
4	Ni	$2.7 \pm .1$	$3.2 \pm .1$	$3.4 \pm .3$	.810
2	Ni	$2.8 \pm .15$	$3.3 \pm .1$	$2.9 \pm .2$	.847

This is a result we still cannot explain. In the rest of the data analysis, we have tried to account for the missing numbers of neutrons.

#### VI. ACCOUNTING FOR LOST NEUTRONS

To try to account for the missing neutrons, we first examined the neutron capture time distributions taken from the Multi-Stop counter for the first  $50\mu\text{s}$  of the  $150\mu\text{s}$  long counting gate; the unit of data size chosen was too small for each of the individual times, so we could only store part of the counting gate. An example of the capture time distributions is shown in Figure 11.

This is data from the Ag Setup #2 run, showing the first, third, and seventh neutron capture times, along with the sum of the first twenty captured neutron distributions. One can see that the capture times for the successive neutrons move slowly to the right. It was thought perhaps that in the higher multiplicity events, we could have been losing neutrons outside of the  $150\mu\text{s}$  long counting gate.

In order to estimate the number of neutrons escaping from the counting gate, we applied a fit to the total neutron capture time distributions (the first twenty neutrons added together) using the functional form<sup>5</sup>

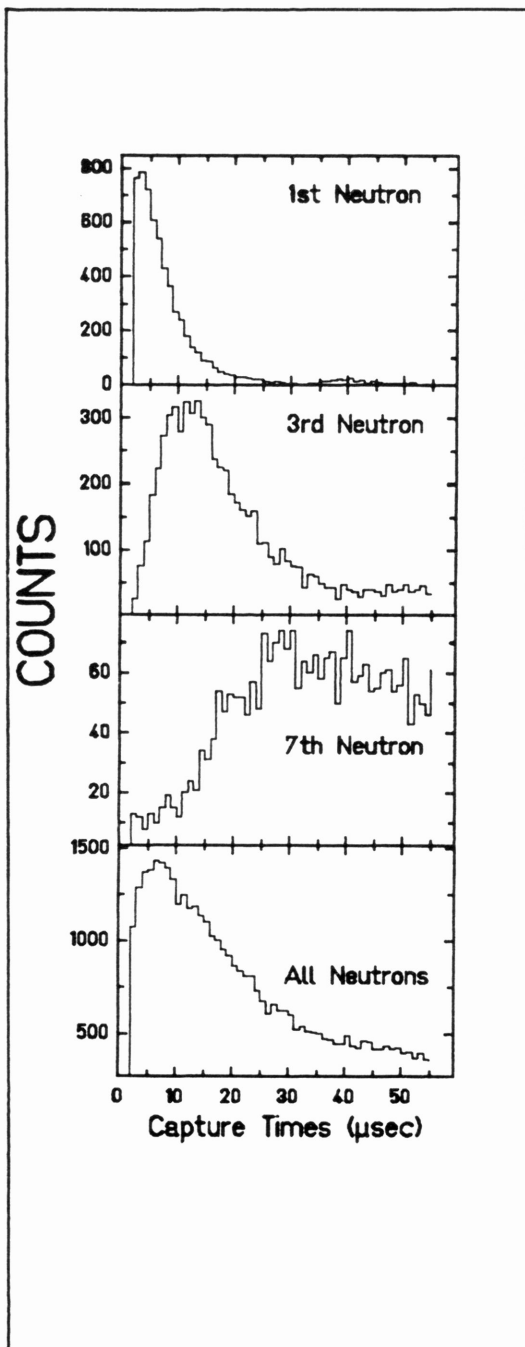


Figure 11. Sample neutron capture time distributions, taken from Ag Setup #2 data.

$$h(t) = N( \exp(-\lambda t) (t(\beta-\lambda)-1) + \exp(-\beta t) ) \quad (3)$$

The three free parameters for the least-squares fit were  $N$ ,  $\beta$ , and  $\lambda$ . The parameter  $\beta$  is directly proportional to the percentage by weight of Gd in the liquid scintillator. While the parameter  $\lambda$  is inversely proportional to the time it takes for the neutrons in the scintillator to reach the thermalized energy.<sup>6</sup>  $N$  acts as a normalization. The total Ni and Ag capture time distributions, with Setups #2 and #4 added together, are shown in Figures 12 and 13, along with a rough plot of the fits using the functional form (3). Table 4. shows the parameter values found for both of the fits.

Table 4.  
Parameter Values for  
Capture Time Distribution Fits

Target	N	$\beta$	$\lambda$
Ni	1589	.0235	2.337
Ag	1626	.0309	1.604

The shape of the two fits is quite different at the higher capture times; they should be fairly close to each other, with the fitting function being more or less reaction independent, assuming the individual capture time distributions can be added

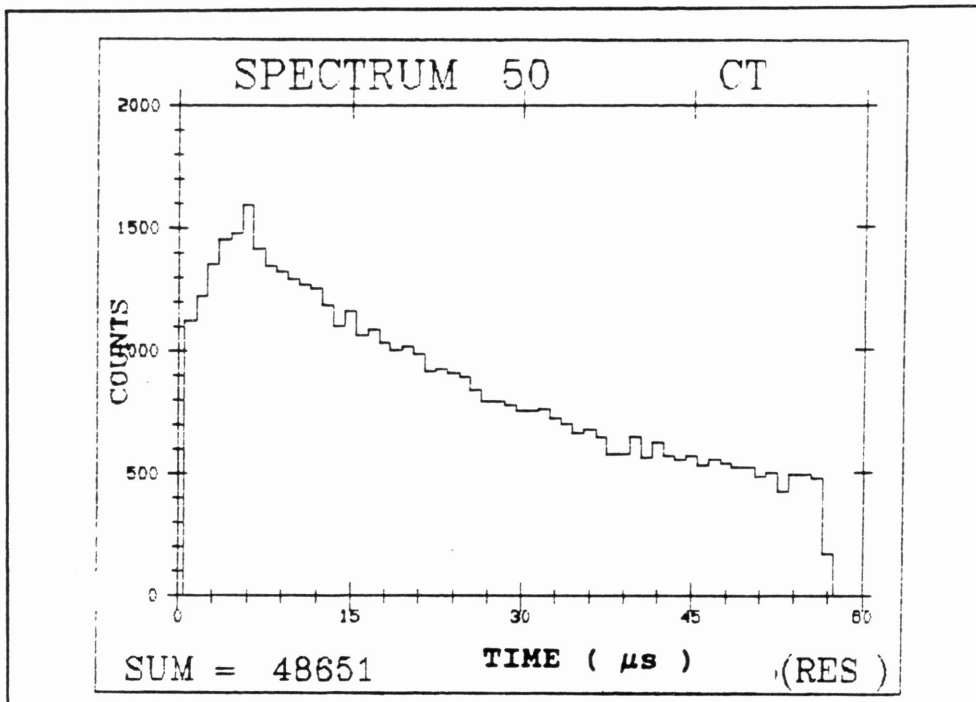


Figure 12a. A plot of the first twenty neutron capture time distributions added together for the Ni Setup #2 data.

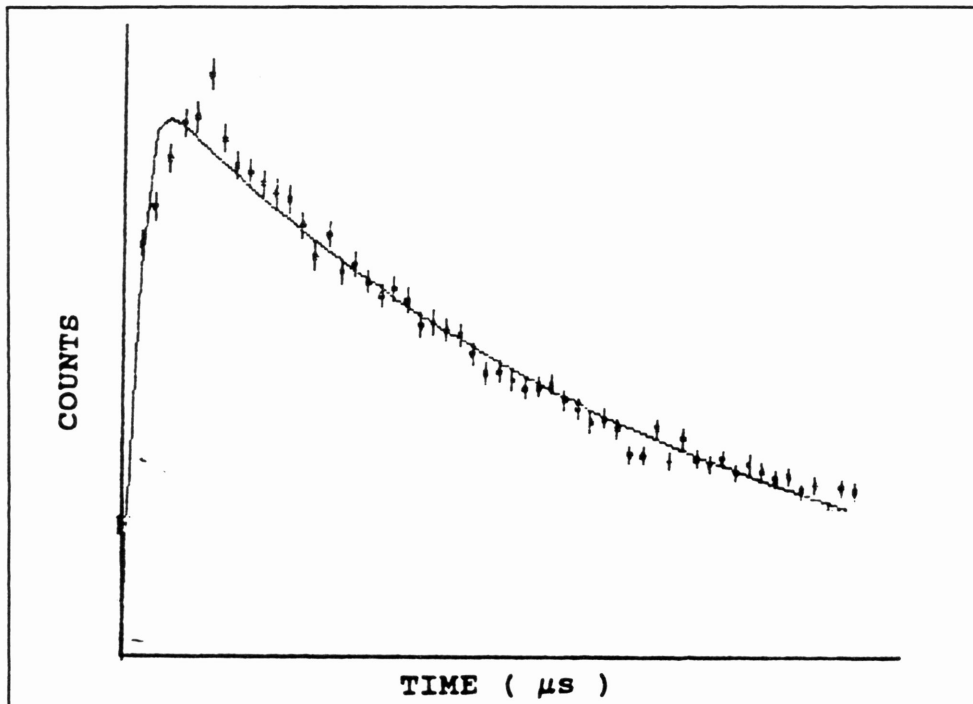


Figure 12b. The fit attempt (linear plot) for Figure 12a.

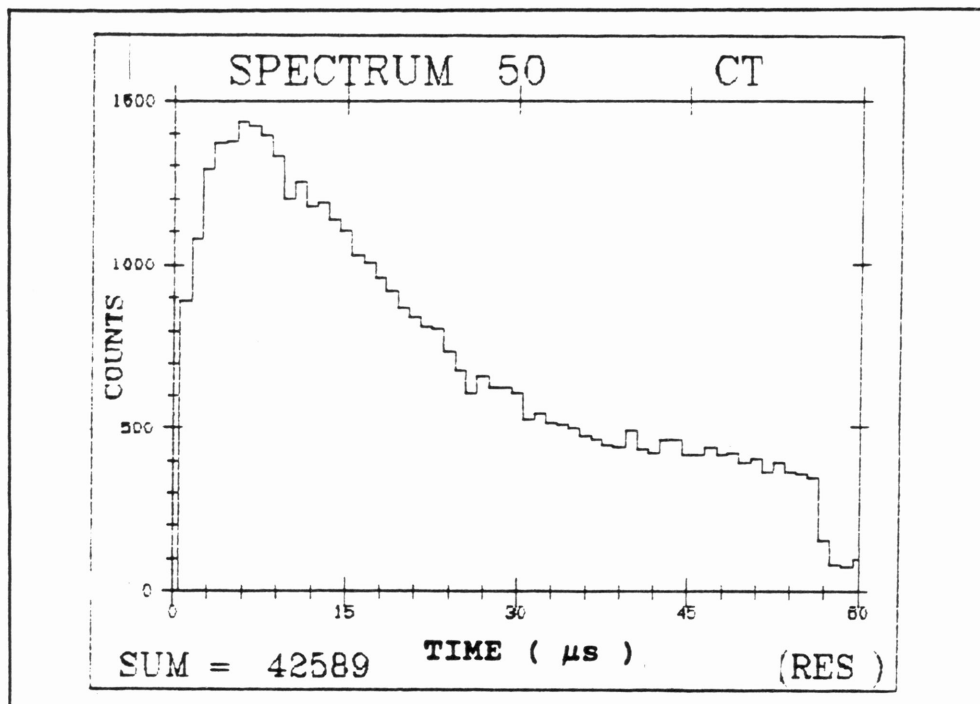


Figure 13a. A plot of the first twenty neutron capture time distributions added together for the Ag Setup #2 data.

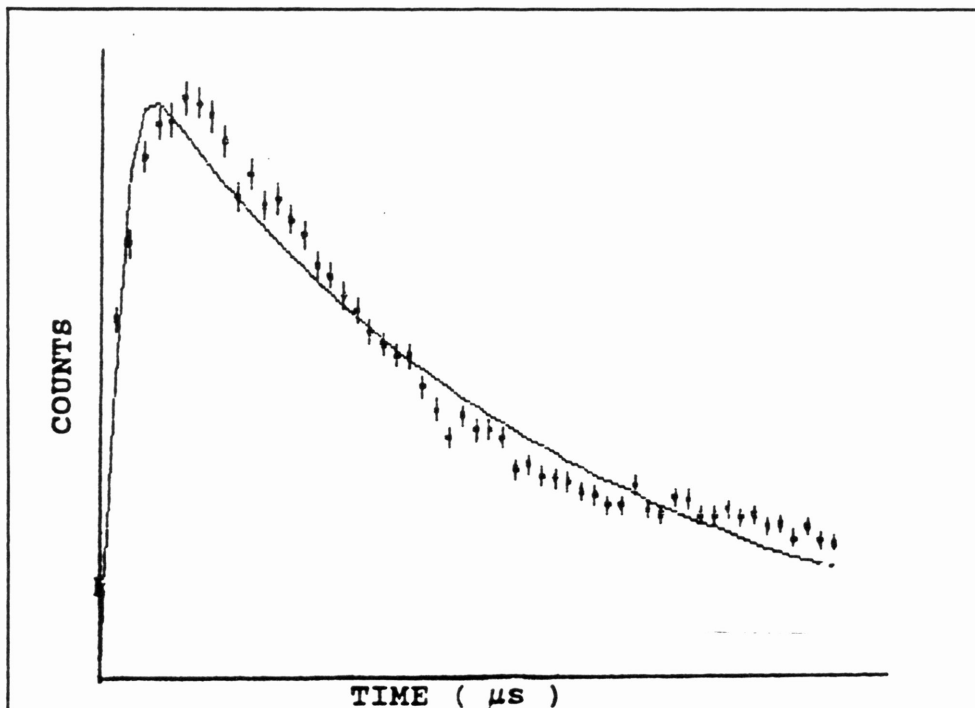


Figure 13b. The fit attempt (linear plot) for Figure 13a.

independently. The two different values of  $\beta$  indicate different concentrations of Gd in the scintillator. We are still unable to explain the results of this fit. After integrating the fitting functions above  $150\mu\text{s}$ , we found that in the nickel and silver cases, we were only losing approximately 3% and 1% of the neutrons respectively, not high enough to account for the missing numbers.

## VII. CONCLUSIONS AND FUTURE PLANS

After studying the capture time distributions, we have still been unable to come up with an explanation for the low neutron counts. The strange second component in the  $^{252}\text{Cf}$  multiplicity distributions is also still unaccounted for. Dr. Natowitz's research group is currently running another test of the Neutron Ball, taking advantage of the brand new ion source at the Cyclotron. This experiment involves beams of  $15\text{ Mev/u } ^{20}\text{Ne}$  and  $35\text{ Mev/u } ^{40}\text{Ar}$  on a  $^{238}\text{U}$  target.

Preliminary analysis of the data indicates the average neutron multiplicities are now in their correct ranges. Several different silicon detectors are being used in the experiment at different angles from the beam direction. Hopefully the experiment will shed some light on the effectiveness of our data analysis scheme, and help us better understand how the Neutron Ball responds in an experiment.

I would like to thank Dr. Natowitz and Dr. Ryoichi Wada for their patience and guidance in seeing me through this project,

and also Dennis Utley who helped me by grinding through a lot of the tougher analysis. Special thanks also goes to Dr. Kris Hagel and Dr. Michel Gonin for providing invaluable advice during the study.

## REFERENCES

1. S.S. Datta, PhD. Thesis (Panjab University, 1987), "Study of Energy Dissipation and Nuclear Deexcitation Mechanism via Exclusive Measurements of Neutron Multiplicity Distributions", University of Rochester reprint (1987) pp. 6-13.
2. R.R. Spencer, R. Gwin, and R. Ingle, Absolute measurement of  $\bar{\nu}_p$  for  $^{252}\text{Cf}$  using the ORNL large liquid scintillator neutron detector, ORNL Report No. ORNL/TM-7940(1979).
3. A. Gauron, Phys. Rev. C 20 (1980) 230.
4. R. Wada, D. Fabris, K. Hagel, G. Nebbia, Y. Lou, M. Gonin, J.B. Natowitz, R. Billerey, B. Cheynis, A. Demeyer, D. Drain, D. Guinet, C. Pastor, J. Alarja, A. Giorni, D. Hever, C. Morand, B. Viano, C. Mazur, C. Ngô, S. Leray, R. Lucas, M. Ribrag, and E. Tomasi, Phys. Rev. C 39 (1989) 497. Also see:  
 K. Hagel, D. Fabris, P. Gonthier, H. Ho, Y. Lou, Z. Majka, G. Mouchaty, M.N. Namboodiri, J.B. Natowitz, G. Nebbia, R.P. Schmitt, G. Viesti, R. Wada, and B. Wilkins, Nucl. Phys. A486 (1988) 429.  
 M. Gonin, L. Cooke, K. Hagel, Y. Lou, J.B. Natowitz, R.P. Schmitt, B. Srivastava, W. Turmel, H. Utsunomiya, R. Wada, G. Nardelli, G. Nebbia, G. Viesti, R. Zanon, B. Fornal, G. Prete, K. Niita, S. Hannuschke, P. Gonthier, and B. Wilkins, "Dynamical Effects on the De-excitation of Hot Nuclei with  $A \approx 160$ ", paper submitted to Phys. Rev. C (1989).
5. U. Jahnke, G. Ingold, D. Hilscher, H. Orf, E.A. Koop, G. Feige, and R. Brandt, in Proceedings of the Symposium on Detectors in Heavy Ion Reactions, Berlin, 1982, Lecture Notes in Physics 178 (Springer Verlag, 1983).
6. J.B. Parker, P. Fieldhouse, L.M. Harrison, and D.S. Mather, Nucl. Instr. and Meth. 60 (1968) 10-11.